ÉCOLE POLYTECHNIQUE
FÉDÉRALE DE LAUSANNE

Modelling cell seeding to homogenize cells distribution within the scaffold for tissue engineering

Ecole Polytechnique Fédérale de Lausanne
Laboratory of Biomechanical Orthopedics

Nathanel Apter

6/18/2015

Cell Seeding is a key factor for good regeneration in tissue engineering. In order to ensure uniform tissue regeneration, a system has to be found to distribute cells evenly within the scaffold that will carry them in the body. In this extent, this work try to find an accurate description of compression forced induced suction which is a seeding technique with reported satisfying seeding efficiency. This description will take the form of a numerical model with COMSOL Multiphysics and will allow us to maximize the seeding in terms of homogeneity. In order to find the best possible seeding, strains and velocities of the compression will be further analyzed. The scaffold material properties will also be examined in order to have the best possible material for that kind of applications.

Table of Contents

1 Introduction

The cartilage is a complex structure that deteriorates with age. Osteoarthritis especially damages the tissue and the actual techniques to replace cartilage as autologous chondrocytes implantation does not bring back the complex network of the cartilage with its properties. To get back the structure of cartilage, scaffolds of polymer containing chondrocytes have been researched.

A cartilage tissue must show homogeneous cell distribution as well as high cell viability. Cells being not evenly distributed within the scaffold may die from hypoxia occurring from the lack of oxygenation of the cells which correlates viability strongly to cell distribution. The distribution will also quantify the quality of the tissue. In this extent, cell seeding techniques for scaffolds need to be improved. Several seeding methods exist nowadays and we can differentiate between static and dynamic seeding. Static techniques based their rearrangement of the cells in the scaffold mainly on static forces as gravity and they do usually not lead good results in term of seeding efficiency (1). Typical static seeding techniques are for example injection seeding using a needle or dropwise seeding using pipette. The results mostly show high cell density in the peripheral parts of the scaffold but low density in the central part and this is exactly what is to avoid.

Dynamical seeding techniques are mostly based on the dynamics of a constant or variable fluid flow inside the scaffold. They normally bring much better seeding efficiency than the static ones.

Perfusion seeding for example uses cyclic flow inside a perfusion chamber to have higher cell distribution inside hydrogel scaffolds. To achieve an oscillating flow several techniques can be used, as an oscillating system using the 2 syringe system (2) or a bioreactor. This bioreactors show high seeding efficiencies: 81-84% (3) however having high variability in seeding efficiency between specimens and other difficulties concerning consistency of the results. Lots of improvements have been done with perfusion chamber, for example using several chambers in cascade to improve the seeding efficiency (4). Perfusion seeding does also bring a good cell viability rate.

Centrifugal seeding and orbital shaker seeding are also dynamical seeding techniques. They show homogeneous distribution however the viability of cells seem to decrease compared with perfusion seeding (2). Centrifuging at a certain specific velocity do even enhance the production of extracellular matrix for mesenchymal stem cells (5). Thevenot and coworkers in their work (6) analyzed the different techniques to access homogeneity of the cells and went through injection, static surface, orbital and centrifuging seeding. They used fluorescence cell staining and cryosectionning to access cell distribution and viability of the different techniques. Orbital seeding as well as centrifuge seeding had good results in terms of efficiency (62% and 55%). Centrifuging however had a really high cell death rate up to 50%.

The seeding technique this report is going to handle is called compression force-induced suction. This technique consists of compressing the scaffold that is embedded in the solution containing cells. When releasing the compression, the pressure difference between the inner of the scaffold and the outside will induce a suction effect (Figure 1) and so force the fluid inside the scaffold. This technique is normally used over several cycles: 5-10 (7). The loading regime can take the cosine form or can follow other shape like the one in Figure 2. To achieve the best possible seeding efficency, the loading regime and the material used need to be optimize and for that purpose it appeared as an evidence to do a numerical model of the compression.

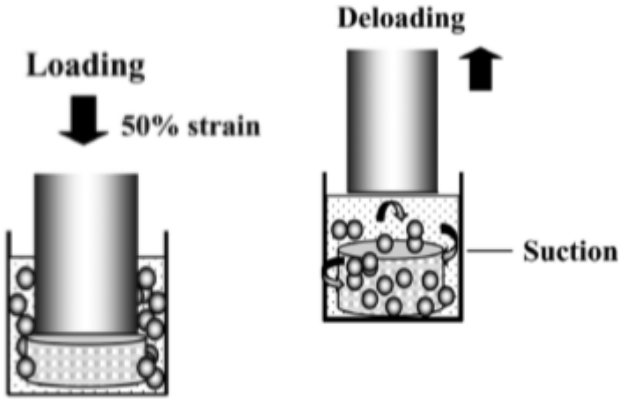

Figure 1: Compression Force-Induced Suction[1]

2 Method

Compression Force induced suction was implemented in COMSOL Multiphysics. For that purpose, it had to be fully described first. Compression Force induced Suction will evenly distribute fluid inside the scaffold only when used at a specific strain rate, a loading velocity and a deloading velocity. To find the best parameters to maximize the seeding an optimization had to performed. First comparing the loading regime, between cosine deformation or linear loading/deloading deformation(Figure 2). Then comparing materials and then comparing the strains, the waiting time and the velocity influence.

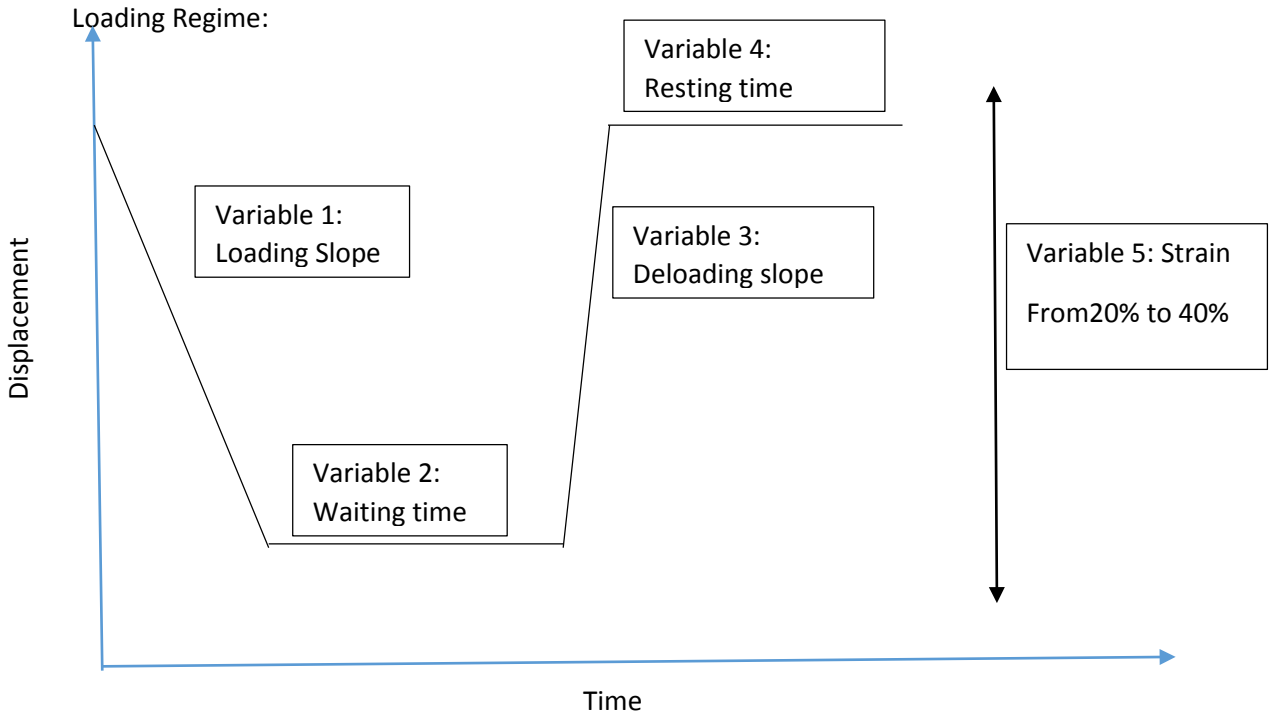

Figure 2: Loading/Deloading Regime

[1] New Technique of Seeding Chondrocytes into Microporous Poly(L-lactide-co-e-caprolactone) Sponge by Cyclic Compression Force–Induced Suction, J.Xie and coworkers

2.1 Geometry

The geometry chosen of the scaffold has cylindrical shape and is 4 mm in radius and 3 mm in thickness (Figure 3).

Figure 3: Scaffolds with different particle size

2.2 Scaffold Characterization

In order to describe the scaffold accurately many assumption had to be done. First the fluid distribution inside the scaffold is assumed to be 2D-axisymmetric, meaning that variation of stress and velocity in angular direction are assumed to be negligible. The fields are always uniform in angular direction so that the stress and velocity. The second assumption is that we can neglect non-linearity as well as viscous behavior of the scaffold which is true for small deformation or for low velocities which represent the range of velocities used. Using these assumptions and knowing that the scaffold is nothing else then a porous structure, the scaffold stress and velocity profile can commonly be described by a special case of the Navier-stokes equation combined with linear elasticity, which is called Biot-poroelasticity (8).

The hydrogel is fully described by the bulk modulus K, the expansion coefficient H and the specific storage coefficient R (9). However the bulk modulus and the expansion coefficient being hard to measure with techniques used nowadays, we choose to replace the description by the common use of the linear elastic theory completed with porosity description which is to the above description. We needed to find values for the porosity, the permeability as well as the Biot-Willis coefficient to have a full description of the scaffolds. The Biot-Willis coefficient (9) is calculated as the bulk modulus K divided by the specific storage coefficient H. It is assumed to be 1 for our case (10). In order to access the other material specific properties, characterization tests were performed.

2.2.1 Scaffold Fabrication

To fabricate scaffolds, we used poly-HEMA(Hydroxyl-ethyl-methacrylate) crosslinked with EGDMA(Ethyleneglycol-Dimethylacrylate). We used different amounts of cross linker to see the influence on the seeding. We used the polymer in form of salt pellets. We also differentiated between fine particles being 100-300µm big and rough particles being 300-500µm big (Figure 3). We mixed 932 µl HEMA with 38 µl ammonium persulfate water solution (100mg/ml), 38 µl sodium metabisulfite water solution (100 mg/ml) and 57.9 µl EGDMA for 4% crosslinker or 86.9 µl for 6% crosslinker. After filtering the solution, we poured the solution in the mold containing salt and thermo-polymerised the samples in the oven at 65°C for 2 hours.

2.3 Boundary Conditions

To implement a numerical model, constrains and boundary conditions had to be chosen.

The scaffold was constrained in z direction in the lower boundary, in order for the scaffold not to move away during the deformation. The problem was calculated in a 2D axisymmetric way and the outer boundary was set free. The pressure at that boundary was set to 0 in order for the pressure differences inside the scaffold to induce a velocity field that would influence the fluid to flow inside or out of the scaffold depending on the pressure gradient.

2.4 Mesh

We used an extra fine mapped mesh constituted of 1900 domains and 176 boundary domains. You can see the mesh in Figure 4(3D-Axisymmetric sketch) with the quality analysis performed by COMSOL. We see that the elements rights at the border of the scaffold have lower quality. In order to ensure good results I did a mesh sensitivity analysis using coarse mesh and extremely fine mesh, obtaining good results for the extra fine mesh.

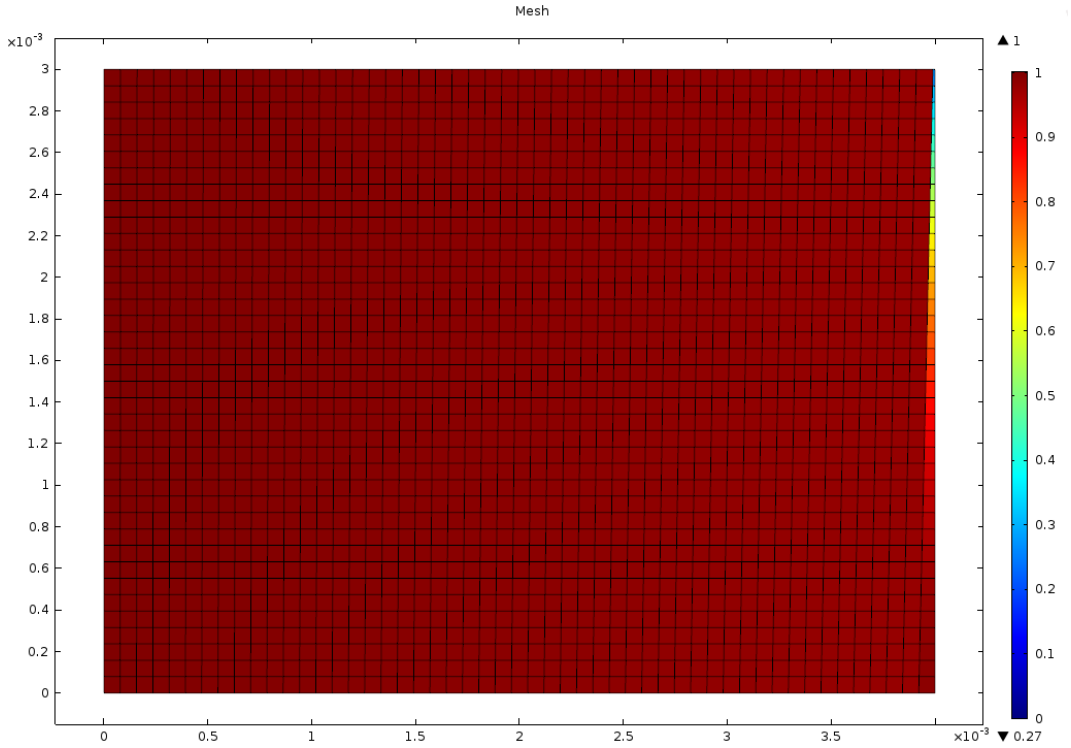

Figure 4: Extra fine mesh of the scaffold with 23793 degrees of freedom.

3 Results and Discussion

3.1 Gel Characterization

3.1.1 Young Modulus

The Young Modulus was calculated using the Force-deformation curve by using a uniaxial loading machine (Instron Loading Machine). The deformation we used to get the force-deformation results were around 40%. By using a speed of 0.1 mm/s, we could assume a linear elastic behavior and neglect the viscous part of the gel as well as the non-linear behavior.

Using the force-deformation curve and following relationships for the stress σ and the strain ε:

$$\sigma = \frac{F}{A} \text{ and } \varepsilon = \frac{l_d - l_o}{l_o}$$

F being the applied force to the scaffold, A the area orthogonal to the applied compression, l_d the thickness at that specific force and l_o the initial thickness. Using Hook's Law for linear elasticity:

$$\sigma = E\varepsilon$$

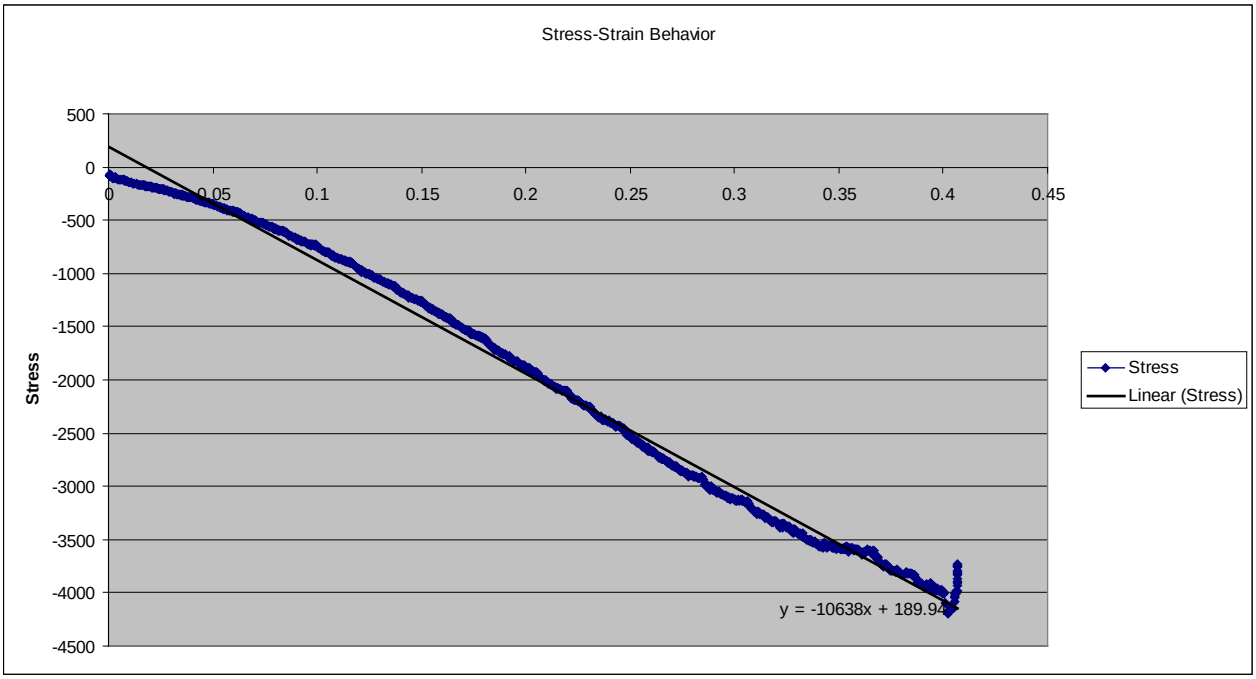

Figure 5: Stress-Strain behavior of a 4% crosslinker fine particle scaffold.

The E-modulus being described as the slope of the curve of the stress-strain behavior(Figure 5). The Stress-Strain curve was computed for 6% and 4% crosslinker scaffolds, for fine and rough particles. The E-modulus seem to increase slightly with the percentage of crosslinker and also inversely to the particle size used to create the scaffold (Figure 6).

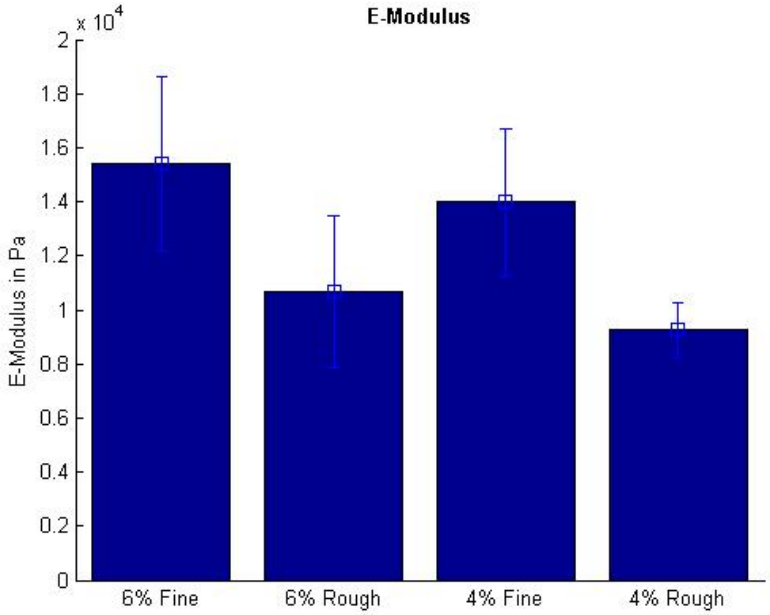

Figure 6: Average Measured E-modulus in Pa with standard deviations

3.1.2 Poisson ratio

The poisson ratio(v) describes the ratio of the strain orthogonal to the deformation to the strain in the direction of the deformation and so quantifies the linear anisotropy of the material.

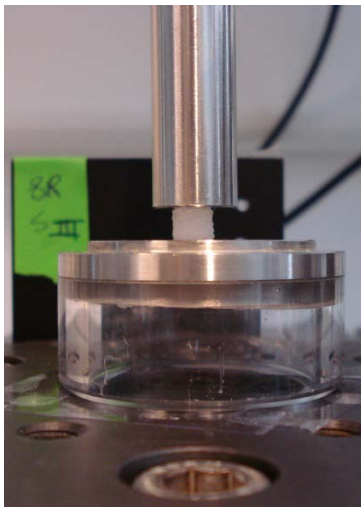

Figure 7: Set-up for poisson ratio measurements

$$\nu = -\frac{d\varepsilon_{orth}}{d\varepsilon_{axial}}$$

For Poisson ratio calculations, we performed compression tests similar to the tests performed for the E-modulus. The set-up is shown in Figure 7. Using a uniaxial loading machine, we applied respectively 20% and 40% strains. We took photos of the samples in the initial state and after deformation and measured the geometries with ImageJ. The results were unsatisfactory in the first try. The samples being too small in thickness, the anisotropy of the material got too important for the measurements. New samples with higher thickness were produced (7mm). These samples brought satisfactory results.

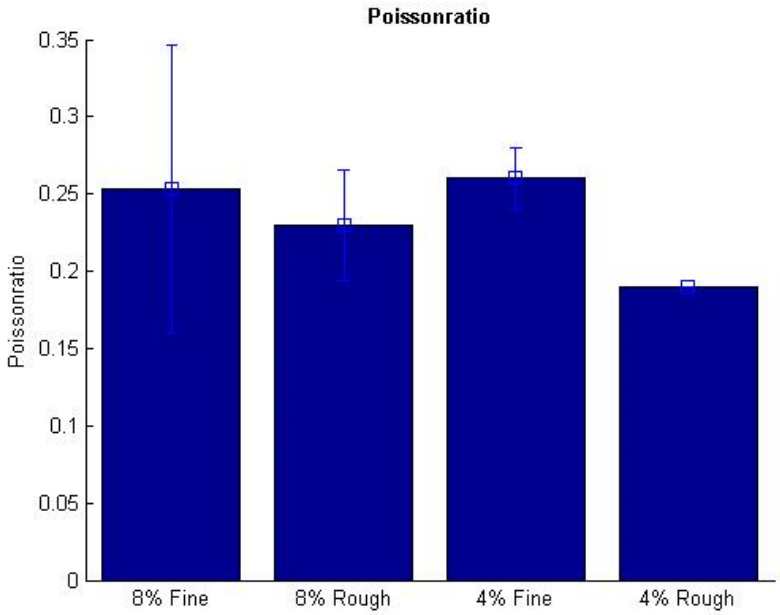

Figure 8: Poisson ratios results for different particle size and amount of crosslinker

3.1.3 Porosity

For the porosity measurements the samples were freezed-dried in liquid nitride and then vacuumed.

We performed MicroCT scans to obtain the porosity of the samples. The MicroCT analyze every layer of the scaffold with x-rays and gets an image of the structure(see Figure 9).

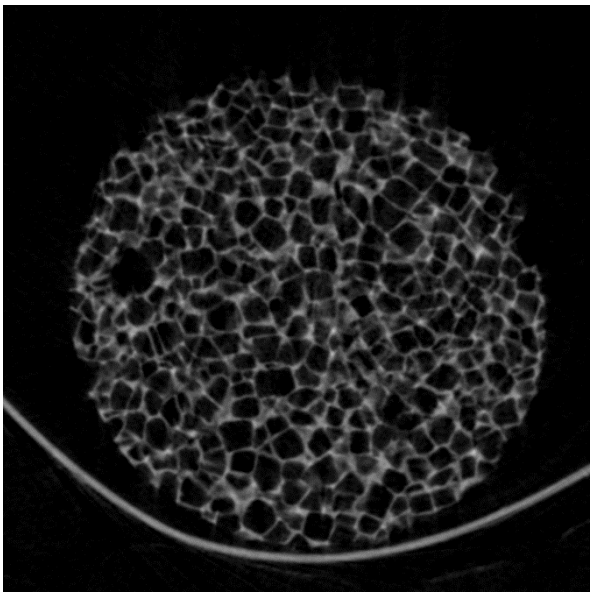

Figure 9: An x-ray image of a 4% crosslinker, fine particles scaffold

The software then computed the porosity by knowing that it is defined by

$$\vartheta = \frac{Liquid\ volume}{Total\ volume}$$

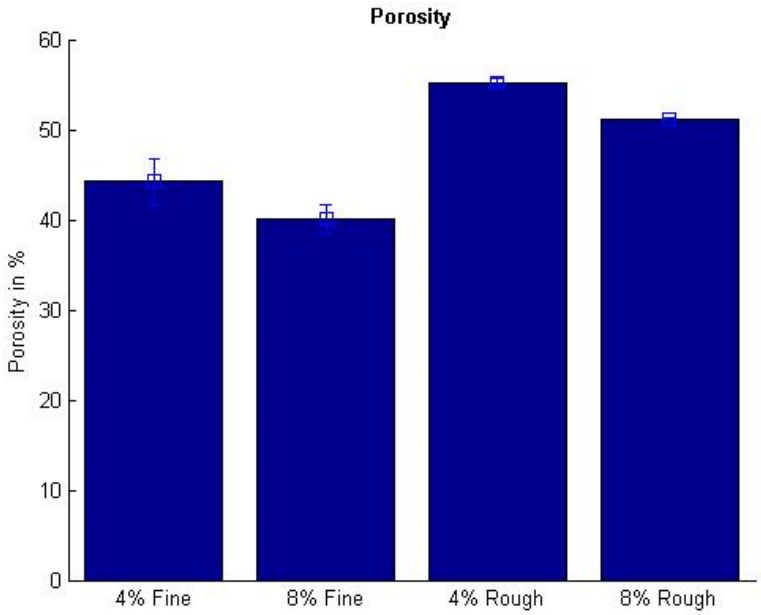

Figure 10: Porosity results for different particle size and amount of crosslinker

We note higher porosity for rougher samples and lower porosity for higher amount of crosslinker. We then implemented the porosity in COMSOL Multiphysics as a strain dependent variable:

$$\varepsilon_p = \frac{\varepsilon_{p0} + \varepsilon_{vol}}{1 + \varepsilon_{vol}}$$

ε_{p0} = Initial Porosity, ε_{vol}= Volumetric Strain

We also used the scans to verify the pore size distribution for rough and fine scaffolds(Figure 11). The distribution was as expected. The distribution of the pores of the rough particles scaffolds was around higher values than for fine particles scaffolds.

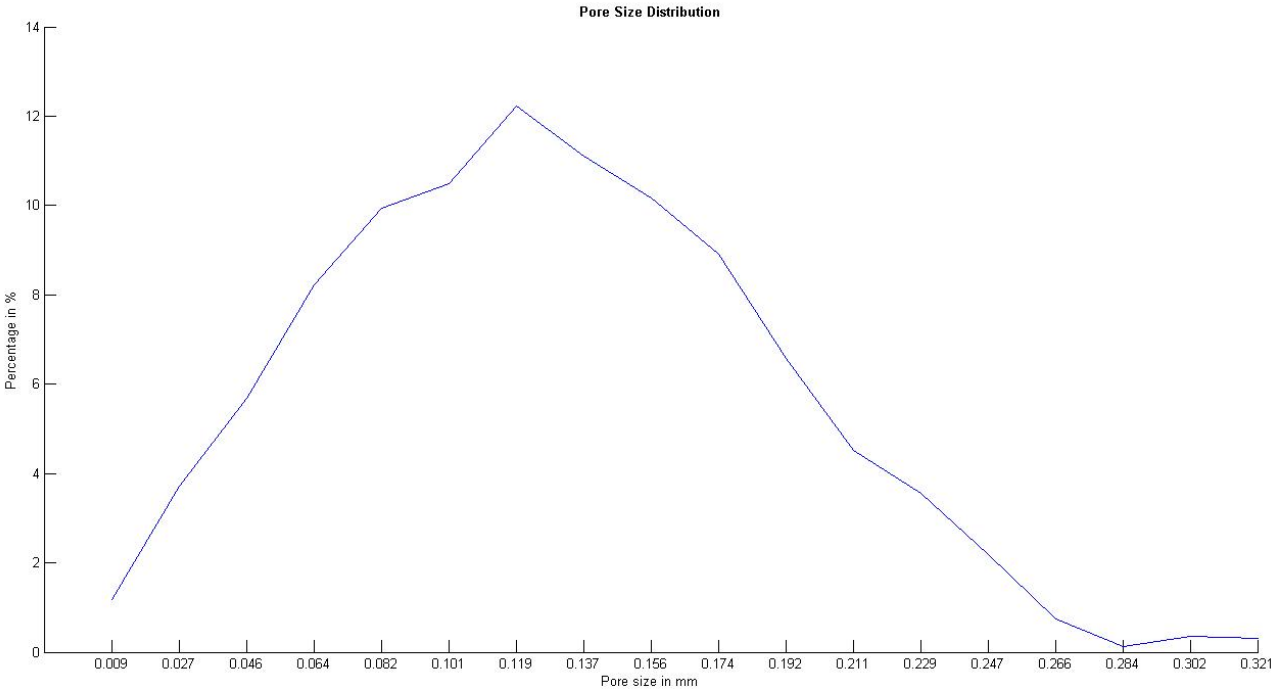

Figure 11: Pore size distribution for a fine particle scaffold, normal distribution around 119µm

3.1.4 Permeability

Permeability is described by the pores properties, the initial permeability can be described for salt leached scaffolds by the Kozeny-Carmen equation (11) that is expressed by:

$$k_0 = \frac{n_A L W^3}{12}$$

for rectangular pores. L being the length of the pores, W the width and n_A is the number of pores per unit area. The strain dependent permeability is then calculated accordingly:

$$k = k_0 \left(\frac{1+e}{1+e_0}\right)^M$$

M:1 to 5 and e:void ratio

The factor M is material dependent. It is however not accessed yet for the scaffold we used. For cartilage it is assumed to be 1.3 and this value was also used in the model (12).

The void ratio being calculated by:

$$e = \frac{\vartheta}{1-\vartheta}$$

We so obtain values for the permeability (Figure 12). Again this material property will be strain dependent, as it is also for cartilage (13). We have to account that, to implement this value in COMSOL Multiphysics.

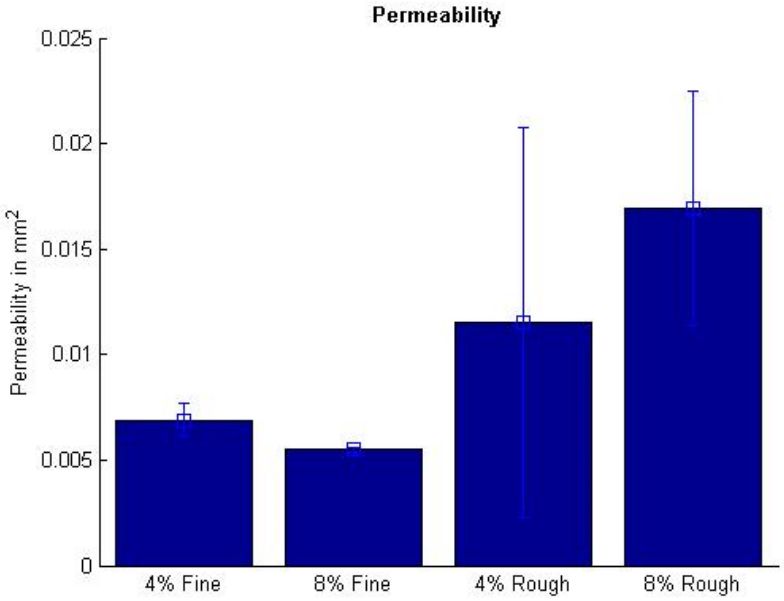

Figure 12: Porosity results for different particle size and amount of crosslinker

We notice high standard deviations for rough samples; however the samples have higher permeability for rough particles.

3.1.5 Density

We also calculated density by doing swelling tests and obtained following results (Figure 13). The density was calculated by calculating scaffolds weight divided by the volume of scaffold. The scaffolds volume was calculated by measuring the scaffolds volume and multiplying it by 1-porosity. The density has similar values for all scaffolds.

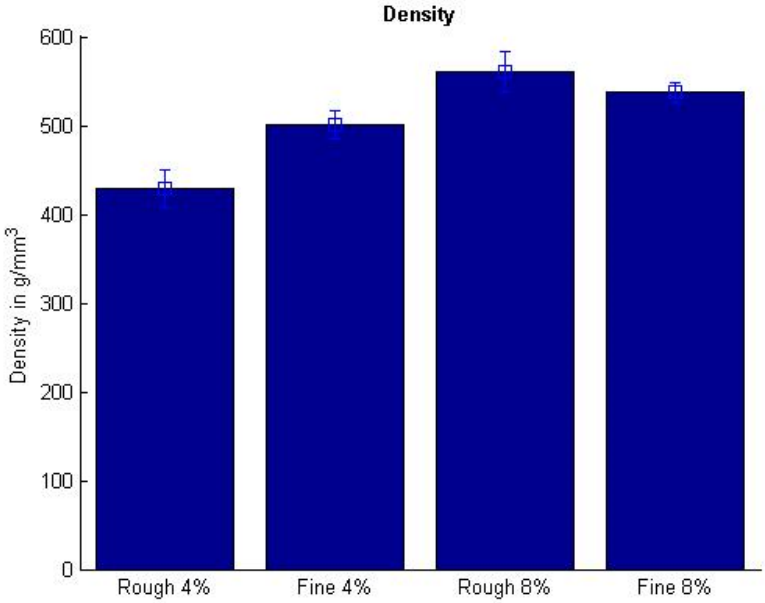

Figure 13: Results for density for different particle size and amount of crosslinker

3.2 Compression Force induced suction

We first performed calculation to find out the best deformations and then probed the effect of particle size and the amount of crosslinker. The default values used to optimize the shape of the deformation were 10 kPa for young modulus, 0.25 for poisson ratio, 50% porosity and 10^{-14} m^4 for the permeability.

We first performed a cosine form deformation because it is mostly used nowadays for cell seeding. To access whether this deformation is efficient we observed the pressure profile with time near the border(3.99mm) of the scaffold on the upper border where the deformation occurs. The negative pressure occurring at that point will mean better penetration of the fluid into the structure. The pressure should be negative for the fluid to be driven inside the scaffold. With high positive pressure lots of fluid will be expelled out of the scaffold what we actually want to avoid.

In Figure 14, you can see cosine deformation using 0.1 Hz frequency. The green deformation shows the pressure evolution for 40% strains and the blue one for 20% strains. The pressure seems to be significant for 20% strains and even more for 40% strains neither.

We then compared the commonly used deformation shape of Figure 2 using different strains and loading and unloading velocities. Using slow unloading velocities as 0.0001m/s, we noticed bad results and much better results for higher velocities as 0.005 m/s. We also varied loading velocities (Figure 15). We note better results for higher strains but also better results for slow loading velocities. The high positive pressures, present at the beginning of the deformation (Figure 15) with high loading velocities were strongly attenuated at slow deformation. We note also that the peaks of pressure of this loading regime are much more enhanced than the ones for cosine deformation.

We also analyzed the effect of putting a time lap between loading and unloading (Figure 16). The break time increases slightly the pressure. In all the Figures, there is to note that pressure is increased with higher strains.

We finally made computations for different material constants. The material constants for various amount of cross linkers and particle size were implemented. The amount of crosslinker did not really influence the results. The particle size was influencing results strongly. The results were much better for small particle size(100-300µm). By comparing Figure 14 and 15 it is obvious that finer particle has better fluid suction inside the scaffold, nevertheless we still have higher removal of fluid during the loading.

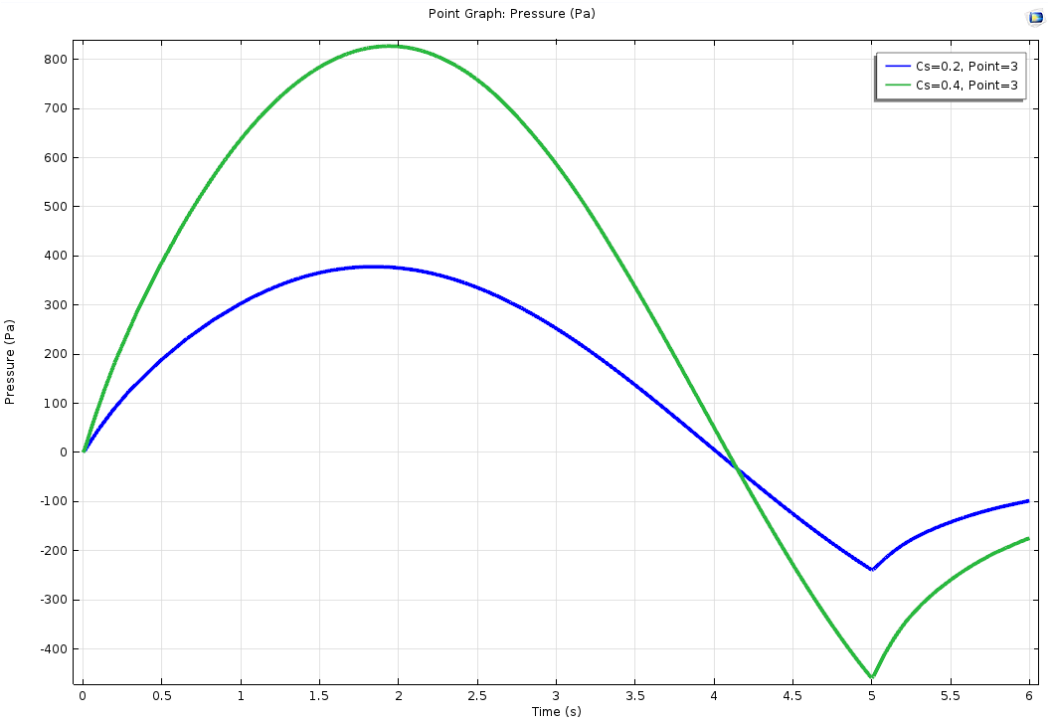

Figure 14: Pressure with time near the free border of the scaffold for cosine deformation for 20% strains(blue) and 40% strains(green)

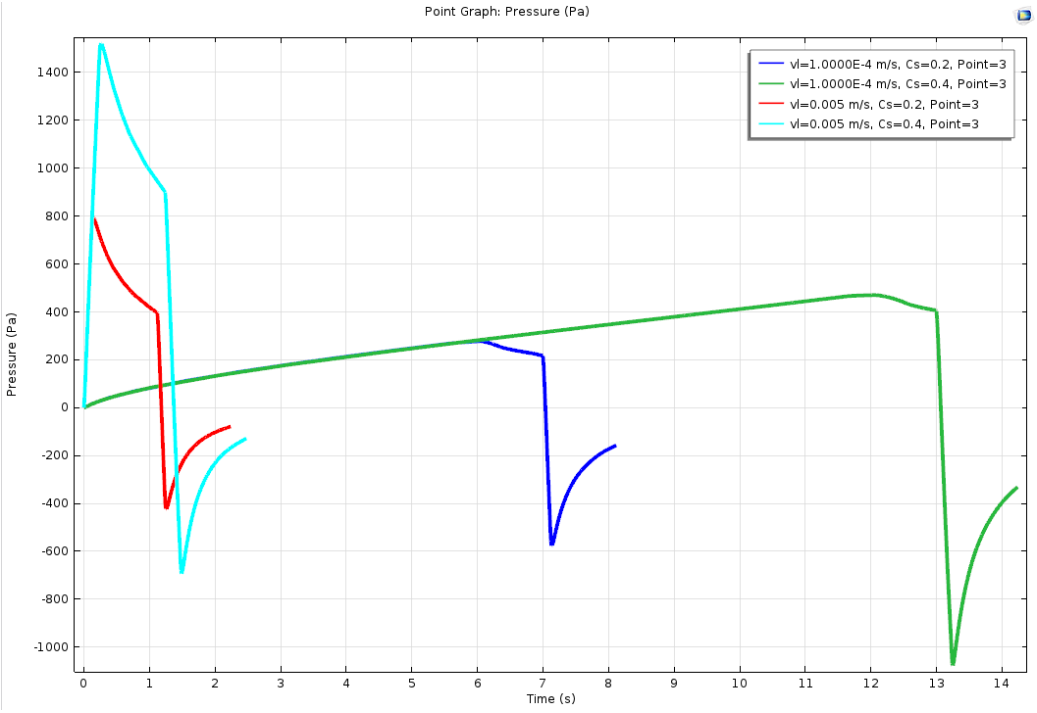

Figure 15: Pressure with time near free border of the border with various loading velocities and strains: 0.005 m/s and 20% strains(red), 0.005 m/s and 40% strains(light blue), 0.0001 m/s and 20% (blue), 0.0001 m/s and 40% strains(green).

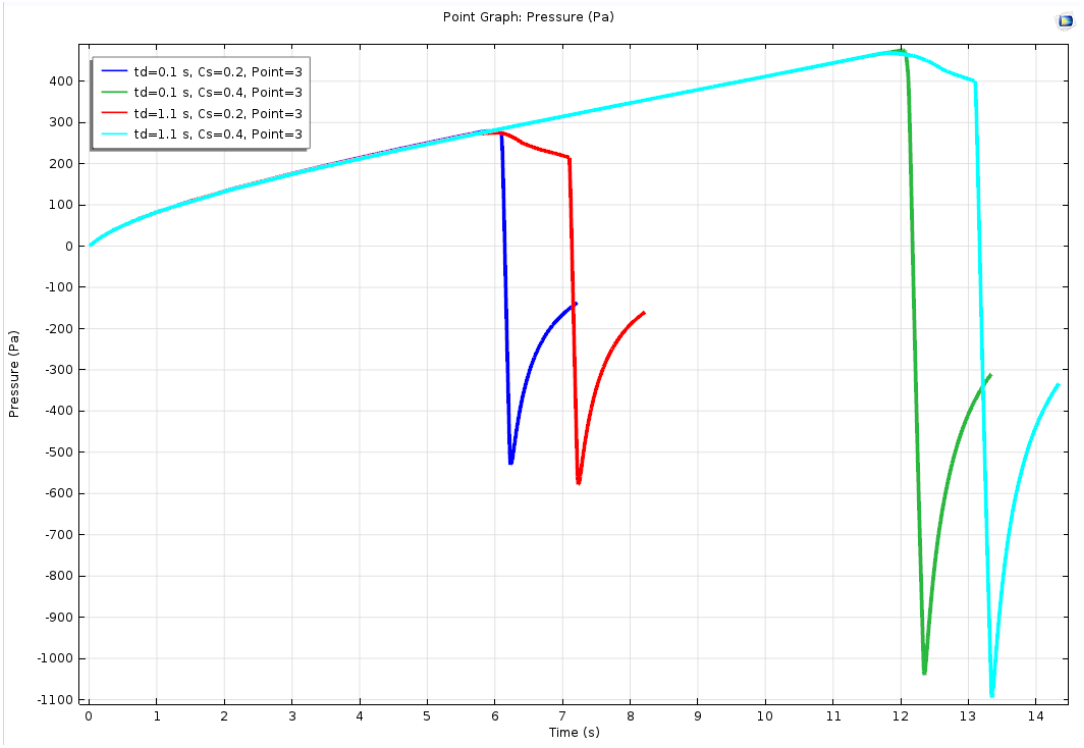

Figure 16: Pressure with time near the free border with various break time between loading and deloading: 0.1s break and 20% strains(blue), 1.1s break and 20% strains(red), 0.1s and 40% strains(green), 1.1s and 40% strains(light blue)

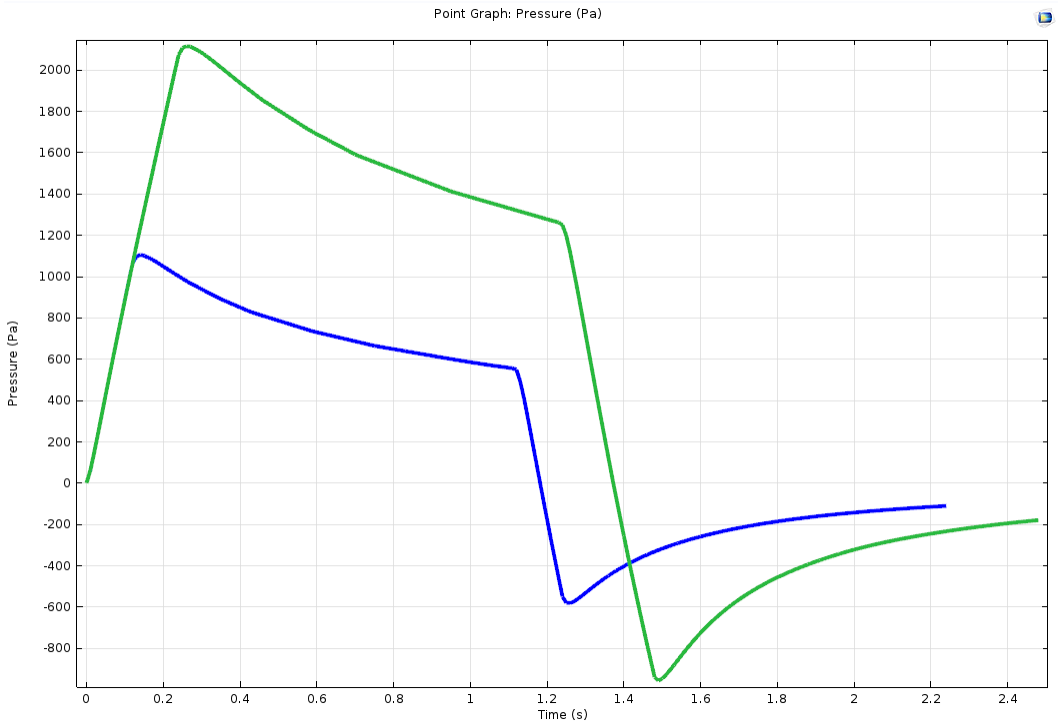

Figure 17: Pressure with time near the free border for scaffold polymerized with fine particles and 4% cross linker: 20% strains(blue), 40% strains(green).

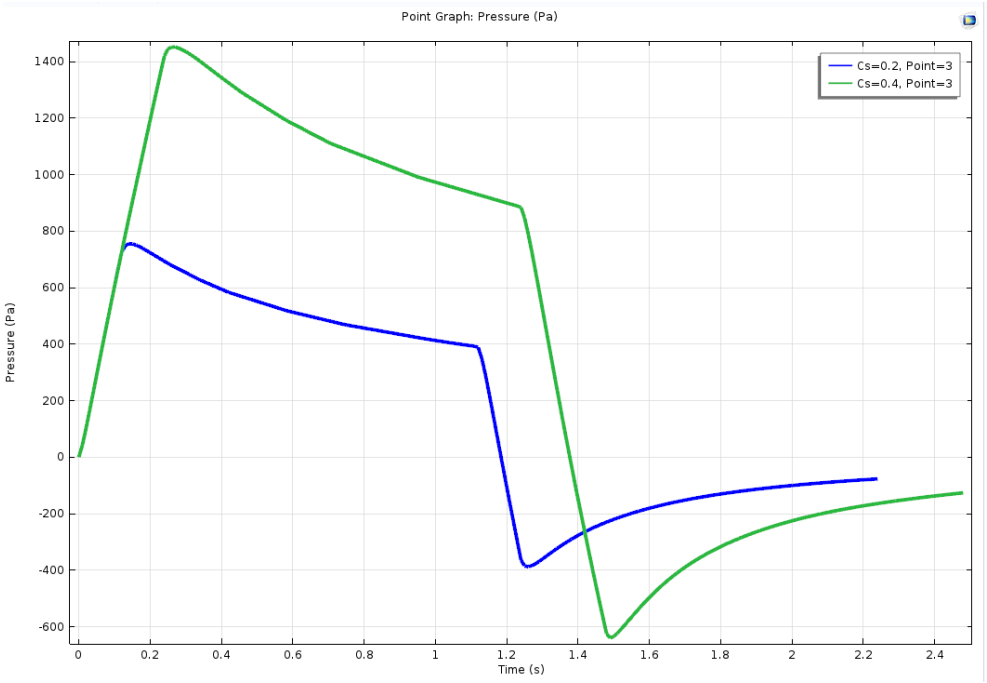

Figure 18: Pressure with time near the free border for scaffold polymerized with rough particles and 4% crosslinker: 20%% strains(blue), 40% strains(green)

3.3 Verification

In order to verify the results, I performed verification using compression force induced suction on real scaffold and using medium and cells(Figure 19). We diluted cells in medium(2 mio in 250 ul medium) and performed seeding for different strains (20% and 40%), unloading velocities 0.1mm/s and 5mm/s and scaffold particle size(rough and fine). After seeding and incubation cell-scaffolds construct 1 hour for cells attachment, 1ml cell culture medium was added to each sample and we incubate them overnight at 37^{o} C and 5% CO condition. Next, MTT staining was conducted according to instructions of the product (Cell Proliferation Kit I (MTT)-Roche Applied Science) in order to assess the living cell distribution inside the scaffold.

Figure 19: Set up for compression force induced suction

The results were sensibly better for faster deloading velocity (5 mm/s) than for slow one (0.1mm/s) as expected by the numerical model(Figure 20). For the strain rate the results are more mitigated. As already mentioned, the pressure appeal allowing cells to penetrate inside the scaffold means also a peak of pressure driving the liquid outside of the scaffold right before (Figure 15). This pressure will be higher for higher strains and so the compensate the pressure driving the fluid inside the scaffold.

Figure 20: Surface of two scaffolds of rough particles seeded with 40% strains and 5mm/s unloading velocity for the one in the left and 0.1mm/s unloading velocity on the right(The black clusters mean cell are just in the surface).

Finally the rough particles scaffolds seem to bring much better results than the fine one(Figure 21). Xie and coworkers (7) did also find out that a higher porosity seem to influence positively the seeding efficiency. This confirms the verification done by compression force induced suction. In terms of mechanics, this simply means that for bigger pores the fluid can enter the scaffold more easily. However, the COMSOL model does not account pore size and interprets the finer structure as a structure having higher stresses for the same deformation because the structure is highly packaged in that case. It would probably be meaningful to either probe this discrepancy experimentally or repeat the simulation using real scans of the structure and a micro FE model to describe the scaffold and not use the poroelastic module which does not consider an accurate description for this particular problem.

Figure 21: Surface of two scaffold seeded with 40% strains and 5 mm/s unloading velocity. The left scaffold being polymerized using fine particles and the right one using rough ones. The black points are the MTT stained cells.

4 Conclusion

The numerical COMSOL model allowed us to make statements about the material properties and the loading regime needed to maximize seeding. Even though, the results are far from ideal and still present deviations from reality, the results seem qualitatively accurate. The problems due to a lack of complete description of the scaffold could probably be decreased by having the 3d scan of a real scaffold instead of a domain defined as poroelastic. It is also important to notice that the results are based on one cycle of compression and that they may be completely different if having 5 to 10 cycles of compression.

Acknowledgements

I would like to thank my supervisor Naser Nasrallahzadeh as well as Alex Terrier, Ulrike Kettenberger as well as Sandra Jaccoud for their great help during my work. I also thank Prof. Pioletti and all other collaborators of the laboratory for biomedical orthopedics for helping me to perform tests and computations.

Bibliography

1. *Flow Perfusion Improves Seeding of Tissue Engineering Scaffolds with Different Architectures.* **J.F.Alvarez-Barreto, S.N.Linehan, R.L.Shambaugh, V.I.Sikavitsas.** March 2007, s.l. : Annuals of Biomedical Engineering, 2006, Vol. Volume 35 Nr. 3.

2. *High-Density Seeding of Myocyte Cells for Cardiac Tissue Engineering.* **M.Radisic, M.Euloth, L.Yang, R.Langer, L.E.Freed, G.Vunjak-Novakovic.** May 20 2003, s.l. : Biotechnology and Bioengineering, 2002, Vol. 82 Nr.4.

3. *Oscillating Perfusion of Cell Suspensions Through Three-Dimensional Scaffolds Enhances Cell Seeding Efficiency and Uniformity.* **D.Wendt, A.Marsano, M.Jakob, M.Heberer, , I.Martin.** Basel : Wiley Interscience, 2003.

4. *Design and Functional Testing of a Multichamber Perfusion Platform for Three-Dimensional Scaffolds.* **M.Piola, M.Soncini, M.Cantini, N,Sadr, G.Ferrario, G.B.Fiore.** s.l. : The scientific world journal, 2013, Vol. Volume 2013.

5. *Centrifugal Seeding Increases Seeding Efficiency and Cellular Distribution of Bone Marrow Stromal Cells in Porous Biodegradable Scaffolds.* **J.D.Roh, G.N.Nelson, B.V.Udelsman, M.P.Brennan, B.Lockhart, P.M.Fong.** New Haven : Tissue Engineering, 2007, Vols. Volume 13 Nr.11, 2007.

6. *Method to Analyze Three-Dimensional Cell Distribution and Infiltration in Degradable Scaffolds.* **P.Thevenot, A.Nair, J.Dey, J.Yang, L.Tang.** Arlington : Tissue Engineering; Part C, 2008, Vols. 14, Nr 4.

7. *New Technique of Seeding Chondrocytes into Microporous Poly(L-lactide-co-e-caprolactone) Sponge by Cyclic Compression Force–Induced Suction.* **J.Xie, Y.Jung, S.H.Kim, T.Matsuda.** s.l. : Tissue Engineering, 2006, Vols. Volume 12, Nr.7.

8. *Mechanics of Deformation and Propagation in porous Media.* **Biot, M.A.** s.l. : Journal of Applied Physics 33, 1962.

9. *Theory of Linear Poroelasticity with Applications to Geomechanics and Hydrogeology.* **H.F.Wang.** 2000, Princeton University Press.

10. *Impact of synovial fluid flow on temperature regulation in knee cartilage.* **M.Nassajian Moghadam, P.Abdel-Sayed, V.Malfroy Camine, D.P.Pioletti.** s.l. : Journal of Biomechanics, 2015, Vol. 48.

11. *Modeling of porous scaffold deformation induced by medium perfusion.* **J.T.Podichetty, S.V.Madihally.** 2014, Oklahoma City : J Biomed Mater, 2014, Vol. Res Part B . 102B:737–748.

12. *A comparison of finite element codes for the solution of biphasic poroelastic problems.* **P.J.Prendergast, W.D Van Driel, J-H Kuiper.** 131-136, s.l. : Journal of Engineering in Medicine, 1997, Vol. 210 no 2 .

13. *Biomechanical properties of human articular cartilage under compressive loads.* **F.Boschetti, G.Pennati, F.Gervaso.** s.l. : IOS Press, 2004 йил, Vols. Biorheology 41 S159-166.